tenuating inflammation in the EAM hearts.

Treatment with ARB or PPARγ increases the circulating APN concentration in humans,[13] although these treatments are unlikely to deliver APN efficiently enough to the severely inflamed myocardium to be clinically relevant. Consistent with our results, previous reports demonstrated that the viral gene delivery of APN or HGF endogenously elevates its concentration in autoimmune myocarditis tissue, leading to immune-modulatory effects and the reversal of LV remodeling.[7,8] In contrast to the in vivo viral transfection method, our cell-sheet-based delivery system eliminates concerns related to the use of plasmid vectors and of needle injection into the host myocardium, and more efficiently delivers multiple cardioprotective factors over the long term.[9,15] After iACS implantation, the expression of cardioprotective factors (APN, HGF and VEGF) in the myocarditis tissues increased significantly, peaking at postoperative day 14, followed by stable and high expression through postoperative day 35. This prolonged and balanced delivery of cardioprotective factors might be more efficient and practical for clinical use than the one-time administration of a single reagent. Moreover, while the transplanted cells and their producing cytokines existed only in the epicardium, functional and pathological recovery by the iACS therapy was detected both in the inflamed and non-inflamed tissues, suggesting that the major therapeutic mechanisms in this study are not direct effects by transplanted cells but paracrine effects by host cardiac cells. The heart is generally formed in contractile myocardium, endocardium and epicardium, and the epicardium is thought to have a rich cardiac progenitor cell niche and to play an important role in cardiac repair.[16]

Notably, it has been shown that cell-sheet implantation into the epicardium induces the expression of multiple cardioprotective factors in the heart, and activates host epicardial cells crucial for cardiac repair. Therefore, these therapeutic effects in the study might be associated with the cell-sheet method. We believe that this "cross-talk" between the transplanted cells and the native myocardium activates and/or inhibits multiple pathways, leading to beneficial effects, and therefore that the cell-sheet method is a rational drug-delivery system for cardiac pathologies.

The T-cell-related immune modulatory effects were different between the EAM hearts treated with iACS vs. SVFCS transplantation in this study. While the level of Th1-producing IFNγ in the inflamed area of the heart on day 21 was lower in the iACS group than the SVFCS group, the level of Th17-produced IL17 was not significantly different between them. In addition, regulatory T cells accumulated prominently and to a similar degree in both the iACS and SVFCS groups. Nonetheless, the acute myocarditis severity on day 21 was significantly less after iACS implantation than after SVFCS implantation. The functional assessment also showed that the RWMI increase from day 7 to day 28 of the acute myocarditis phase was less in rats receiving iACS implantation than SVFCS implantation. Thus, the acute myocarditis severity on day 21 might be mainly associated with the Th1-mediated autoimmune response. In contrast, iACS implantation significantly elevated the level of APN in the myocarditis tissue, compared with SVFCS implantation. A T-cell proliferation assay showed that the addition of iACS supernatant, which contained APN and HGF, significantly decreased the level of Th1-producing IFNγ, compared with the addition of recombinant HGF alone. These findings indicated that the greater immunosuppressive effects of iACS implantation on effector Th1 cells compared with SVFCS implantation might be associated with the synergistic paracrine effects of APN and HGF released by the implanted iACS.

Regulatory T cells and effector Th17 cells might be reciprocally regulated in various autoimmune diseases.[3] In our study, some reciprocity between the number of accumulated Foxp3 regulatory T cells and the amount of IL17-producing Th17 in the myocarditis tissues was observed among the groups. ELISA analysis of the myocarditis tissues on day 21 showed that the iACS and SVFCS implantation similarly suppressed Th17 cells and activated the Foxp3 regulatory T cells. Recently, Baldeviano et al. reported that Th17-produced IL17 was dispensable for the severity of the acute myocarditis, but essential for the progression of cardiomyopathy.[3] Consistent with this, we found that the cardiac fibrosis related to LV remodeling in the chronic cardiomyopathy phase was similarly attenuated in the iACS and SVFCS implantation-treated rats via the suppression of profibrotic factors: TGFβ, MMP2, and MMP9. Thus, this inhibition of morphological deterioration might be associated with the suppression of the Th17-mediated autoimmune response and the induction of immune tolerance. In accordance with this scenario, morphological LV remodeling, such as LV dilatation and LV thinness, on day 42 was similarly suppressed in the groups receiving iACS and SVFCS implantation. In addition, the assessment of RWMI showed that the LV functional deterioration from day 28 to day 56 of the chronic cardiomyopathy phase was similarly suppressed in the rats receiving iACSs and SVFCSs, compared with the Sham operation. However, the cardiac hypertrophy on day 42 was attenuated only in the group receiving the iACSs. Several lines of evidence have indicated that APN directly affects injured myocytes via its receptor, eliciting anti-hypertrophic effects in a pressure-overload hypertrophic model.[13,17] Thus, the significant suppression of hypertrophy in iACS implantation-treated rats might have resulted from direct and synergistic effects of APN and HGF on the injured myocytes, and not from indirect immune modulatory effects via effector Th17 cells.

This study showed that iACS implantation had beneficial immunologic, pathologic, and functional effects on the heart of rats with autoimmune-associated myocarditis. However, in the clinical setting, fulminant myocarditis is etiologically highly heterogeneous, and thus, the autoimmune activity associated with it varies. The effectiveness of the iACS treatment shown in this study is therefore not directly translatable to the clinical situation. The investigation of T-cell activity by cardiac biopsy or circulating blood samples from patients with fulminant myocarditis might be useful for identifying responders or determining whether iACS treatment is indicated.

Normally, human myocarditis has a sudden onset and it has been known that it often follows a rapidly deteriorating course, leading to severe cardiac dysfunction. It has been reported that early diagnosis and subsequent treatment for fulminant myocarditis might be essential in clinical practice.[1] Therefore, methods need to be developed for promptly generating autologous iACS to maximize its therapeutic effects. The use of allogeneic iACS might be an option for clinical applications. Although there are immunologic concerns associated with the use of allogeneic iACS, this study suggested that iACS treatment upregulated APN and HGF, which attenuated the immunological response by inhibiting macrophages and activating regulatory T cells. Moreover, APN can limit allograft rejection by suppressing the expression of local cytokine/chemokine ligands that mediate inflammation and immune-cell recruitment.[18] Thus, the need for immunosuppressive medications might be minimal for allogeneic iACS treatment, although further study is needed.

Conclusions

This study clearly revealed that adipocyte-produced APN and HGF exert significant immunosuppressive effects, not only on Th1 cells, but also on Th17 cells in a typical model of autoimmune disorders. In addition, this tissue-engineered iACS improved the cardiac performance of autoimmune myocarditis via the suppression of autoimmune cellular activity, induction of immune-tolerance, and reversal of LV remodeling. This strategy of using a tissue-engineered drug-delivery system might be applicable to clinical treatments for fulminant myocarditis.

Acknowledgments

We thank Ms Masako Yokoyama and Mr Akima Harada for their technical assistance. We also thank Mr Norikazu Maeda and Mr Iichiro Shimomura for helpful discussions. This study was financially supported by a Grant-in-Aid from the Japan Society for the Promotion of Science (A22659251).

Disclosures

There were no competing interests.

References

1. Gupta S, Markham DW, Drazner MH, Mammen PP. Fulminant myocarditis. *Nat Clin Pract Cardiovasc Med* 2008; **5:** 693–706.
2. Cihakova D, Rose NR. Pathogenesis of myocarditis and dilated cardiomyopathy. *Adv Immunol* 2008; **99:** 95–114.
3. Baldeviano GC, Barin JG, Talor MV, Srinivasan S, Bedja D, Zheng D, et al. Interleukin-17A is dispensable for myocarditis but essential for the progression to dilated cardiomyopathy. *Circ Res* 2010; **106:** 1646–1655.
4. Yu F, Chen R, Takahashi T, Sumino H, Morimoto S, Nakahashi T, et al. Candesartan improves myocardial damage in obese mice with viral myocarditis and induces cardiac adiponectin. *Int J Cardiol* 2008; **129:** 414–421.
5. Choi JO, Yun SH, Sung K, Lee YT, Park JI, Ju ES, et al. Thioredoxin, adiponectin and clinical course of acute fulminant myocarditis. *Heart* 2011; **97:** 1067–1073.
6. Kunita E, Yamamoto H, Kitagawa T, Ohashi N, Utsunomiya H, Oka T, et al. Association between plasma high-molecular-weight adiponectin and coronary plaque characteristics assessed by computed tomography angiography in conditions of visceral adipose accumulation. *Circ J* 2012; **76:** 1687–1696.
7. Bobbert P, Scheibenbogen C, Jenke A, Kania G, Wilk S, Krohn S, et al. Adiponectin expression in patients with inflammatory cardiomyopathy indicates favourable outcome and inflammation control. *Eur Heart J* 2011; **32:** 1134–1147.
8. Futamatsu H, Suzuki J, Mizuno S, Koga N, Adachi S, Kosuge H, et al. Hepatocyte growth factor ameliorates the progression of experimental autoimmune myocarditis: A potential role for induction of T helper 2 cytokines. *Circ Res* 2005; **96:** 823–830.
9. Imanishi Y, Miyagawa S, Meaeda N, Fukushima S, Kitagawa-Sakakida S, Daimon T, et al. Induced adipocyte cell-sheet ameliorates cardiac dysfunction in a mouse myocardial infarction model: A novel drug delivery system for heart failure. *Circulation* 2011; **124**(Suppl 1)**:** S10–S17.
10. Lang RM, Bierig M, Devereux RB, Flachskampf FA, Foster E, Pellikka PA, et al. Recommendations for chamber quantification: A report from the American Society of Echocardiography's Guidelines and Standards Committee and the Chamber Quantification Writing Group, developed in conjunction with the European Association of Echocardiography, a branch of the European Society of Cardiology. *J Am Soc Echocardiogr* 2005; **18:** 1440–1463.
11. Eriksson U, Ricci R, Hunziker L, Kurrer MO, Oudit GY, Watts TH, et al. Dendritic cell-induced autoimmune heart failure requires cooperation between adaptive and innate immunity. *Nat Med* 2003; **9:** 1484–1490.
12. Robinson K, Prins J, Venkatesh B. Clinical review: Adiponectin biology and its role in inflammation and critical illness. *Crit Care* 2011; **15:** 221 (1–9).
13. Shibata R, Ouchi N, Murohara T. Adiponectin and cardiovascular disease. *Circ J* 2009; **73:** 608–614.
14. Yin WH, Wei J, Huang WP, Chen JW, Young MS, Lin SJ. Prognostic value of circulating adipokine levels and expressions of adipokines in the myocardium of patients with chronic heart failure. *Circ J* 2012; **76:** 2139–2147.
15. Shimizu T, Sekine H, Yamato M, Okano T. Cell sheet-based myocardial tissue engineering: New hope for damaged heart rescue. *Curr Pharm Des* 2009; **15:** 2807–2814.
16. Zhou B, Ma Q, Rajagopal S, Wu SM, Domian I, Rivera-Feliciano J, et al. Epicardial progenitors contribute to the cardiomyocyte lineage in the developing heart. *Nature* 2008; **454:** 109–113.
17. Shibata R, Ouchi N, Ito M, Kihara S, Shiojima I, Pimentel DR, et al. Adiponectin-mediated modulation of hypertrophic signals in the heart. *Nat Med* 2004; **10:** 1384–1389.
18. Okamoto Y, Christen T, Shimizu K, Asano K, Kihara S, Mitchell RN, et al. Adiponectin inhibits allograft rejection in murine cardiac transplantation. *Transplantation* 2009; **88:** 879–883.

Supplementary Files

Supplementary File 1

Supplementary Methods

Supplementary File 2

Table S1. Hemodynamic indices 5 weeks after the operation

Table S2. PCR primers used in real-time RT-PCR

Figure S1. T-cell proliferation assay.

Figure S2. Capillary formation on postoperative day 35 in each group.

Figure S3. Quantitative reverse transcription polymerase chain reaction (RT-PCR) results for profibrotic markers: TGFβ, TIMP1, TIMP2, TIMP3, MMP2, and MMP9, respectively (n=12 each).

Please find supplementary file(s);
http://dx.doi.org/10.1253/circj.CJ-14-0840

Biomaterials 35 (2014) 7839–7850

Contents lists available at ScienceDirect

Biomaterials

journal homepage: www.elsevier.com/locate/biomaterials

Excitation propagation in three-dimensional engineered hearts using decellularized extracellular matrix

Haruyo Yasui [a], Jong-Kook Lee [b, *], Akira Yoshida [a], Teruki Yokoyama [a], Hiroyuki Nakanishi [a], Keiko Miwa [b], Atsuhiko T. Naito [d], Toru Oka [a], Hiroshi Akazawa [d], Junichi Nakai [e], Shigeru Miyagawa [c], Yoshiki Sawa [c], Yasushi Sakata [a], Issei Komuro [d, *]

[a] Department of Cardiovascular Medicine, Osaka University Graduate School of Medicine, Japan
[b] Department of Cardiovascular Regenerative Medicine, Osaka University Graduate School of Medicine, 2-2 Yamada-oka, Suita 565-0871, Japan
[c] Department of Cardiovascular Surgery, Osaka University Graduate School of Medicine, Japan
[d] Department of Cardiovascular Medicine, The University of Tokyo Graduate School of Medicine, 7-3-1 Hongo, Bunkyo-ku, Tokyo 113-8655, Japan
[e] Saitama University Brain Science Institute, Japan

ARTICLE INFO

Article history:
Received 16 May 2014
Accepted 28 May 2014
Available online 20 June 2014

Keywords:
Cardiac tissue engineering
Organ culture
ECM (extracellular matrix)
Scaffold
Electrophysiology

ABSTRACT

Engineering of three-dimensional (3D) cardiac tissues using decellularized extracellular matrix could be a new technique to create an "organ-like" structure of the heart. To engineer artificial hearts functionally comparable to native hearts, however, much remain to be solved including stable excitation-propagation. To elucidate the points, we examined conduction properties of engineered tissues. We repopulated the decellularized hearts with neonatal rat cardiac cells and then, we observed excitation-propagation of spontaneous beatings using high resolution cameras. We also conducted immunofluorescence staining to examine morphological aspects. Live tissue imaging revealed that GFP-labeled-isolated cardiac cells were migrated into interstitial spaces through extravasation from coronary arteries. Engineered hearts repopulated with Ca^{2+}-indicating protein (GCaMP2)-expressing cardiac cells were subjected to optical imaging experiments. Although the engineered hearts generally showed well-organized stable excitation-propagation, the hearts also demonstrated arrhythmogenic propensity such as disorganized propagation. Immunofluorescence study revealed randomly-mixed alignment of cardiomyocytes, endothelial cells and smooth muscle cells. The recellularized hearts also showed disarray of cardiomyocytes and markedly decreased expression of connexin43. In conclusion, we successfully demonstrated that the recellularized hearts showed dynamic excitation-propagation as a "whole organ". Our strategy could provide prerequisite information to construct a 3D-engineered heart, functionally comparable to the native heart.

1. Introduction

Heart diseases are one of the leading causes of mortality worldwide [1]. Despite of recent progress in heart failure treatment, heart transplantation is still considered the final destination therapy for patients with end-stage heart failure refractory to conventional therapies. However, the benefits of heart transplantation are limited due to the shortage of donor hearts. In this context, myocardial regeneration therapy has emerged as a new therapeutic approach to treat severe heart failure. Although several clinical trials have been conducted [2], most therapies involved repairing specific regions of the heart and not the entire heart. Large-scale replacement of cardiac cells is a prerequisite for effective treatment of end-stage heart failure.

For this purpose, a new technique for engineering three-dimensional (3D) organ-like tissue using decellularized extracellular matrix (ECM) was reported for the heart [3], lung [4,5], kidney [6,7], and liver [8]. This technique has already been applied clinically for the engineering of airway [9] or heart valves [10]. A recent paper showed that induced pluripotent stem cell-derived cardiovascular progenitor cells repopulated in a decellularized heart and successfully proliferated, then differentiated into cardiovascular cells [11]. This paper also demonstrated that repopulated induced pluripotent stem cell-derived cells exhibited contraction and electrical activity, but reconstructed heart function was evaluated in the small regions of the heart. To date, only limited information is available regarding the function of a totally engineered organ.

* Corresponding authors.
E-mail address: jlee@cardiology.med.osaka-u.ac.jp (J.-K. Lee).

http://dx.doi.org/10.1016/j.biomaterials.2014.05.080
0142-9612/

Evaluation of arrhythmogenicity as a whole organ will be indispensable to construct a functionally comparable 3D engineered heart. In the present study, we hypothesized that recellularized hearts show well-organized conduction as native hearts. To elucidate the point, we investigated excitation–propagation properties of the recellularized heart by live imaging system using Ca^{2+}-indicating protein (GCaMP2) [31].

2. Materials and methods

2.1. Animals

The study was carried out under the supervision of the Animal Research Committee of Osaka University and in accordance with the Japanese Act on Welfare and Management of Animals. The experimental protocol was approved by the Animal Care and Use Committee of the Osaka University Graduate School of Medicine.

2.2. Perfusion and decellularization of rat hearts

Adult female Wistar rats (10–12-weeks-old) were anesthetized and systemic heparinization was followed by a median sternotomy. After ligating the caval veins, the heart was removed from the chest. A 2-mm cannula was inserted into the ascending aorta to enable Langendorff antegrade coronary perfusion. The right atrium was opened and an incision was made to create an atrial septal defect followed by the ligation of pulmonary artery and veins. Heparinized PBS containing 10 μM ATP was perfused for 15–30 min, followed by perfusion with 0.5% sodium dodecyl sulfate (SDS) in deionized water overnight. After washing with deionized water for 15 min, the heart was perfused with 1% Triton-X100 in deionized water for 30 min, followed by washing with antibiotic-containing PBS (100 U/ml penicillin (Invitrogen, Carlsbad, CA, USA), 100 μg/mL streptomycin (Invitrogen) and 1.25 μg/mL amphotericin B (Sigma–Aldrich, St. Louis, MO, USA)).

2.3. Isolation and preparation of rat neonatal cardiac cells

One-day-old neonatal pups were sacrificed. Their hearts were removed and placed immediately into a Petri dish containing Hank's Balanced Salt Solution (HBSS) on ice. After removing the connective tissue, the hearts were minced with scissors or blades. Trypsin (Neonatal Cardiomyocyte Isolation System, Worthington Biochemical Corporation, Lakewood, NJ, USA) was added to the dish to a final concentration of 50 μg/mL, and incubated overnight at 4 °C. Then, trypsin inhibitor reconstituted with HBSS and collagenase reconstituted with L-15 medium were added to the dish. The tissue was placed in a 37 °C shaker bath for about 35 min. The tissue was then strained through a 100-μm cell strainer and washed with L-15 medium 3 times. After centrifuging the tissue, the pellet was collected and resuspended in 30 mL of M199 (Invitrogen) with 10% FBS (BioWest, Kansas City, MO, USA), 100 U/mL penicillin (Invitrogen), 100 μg/mL streptomycin (Invitrogen), and EGM-2 Single Quots (CC-4176, Lonza, Allendale, NJ, USA) except FBS and GA-1000.

2.4. Recellularization of decellularized hearts

Approximately 1.0×10^8 cells were suspended in M199 (Invitrogen) with 10% FBS (BioWest), 100 U/mL penicillin (Invitrogen), 100 μg/mL streptomycin

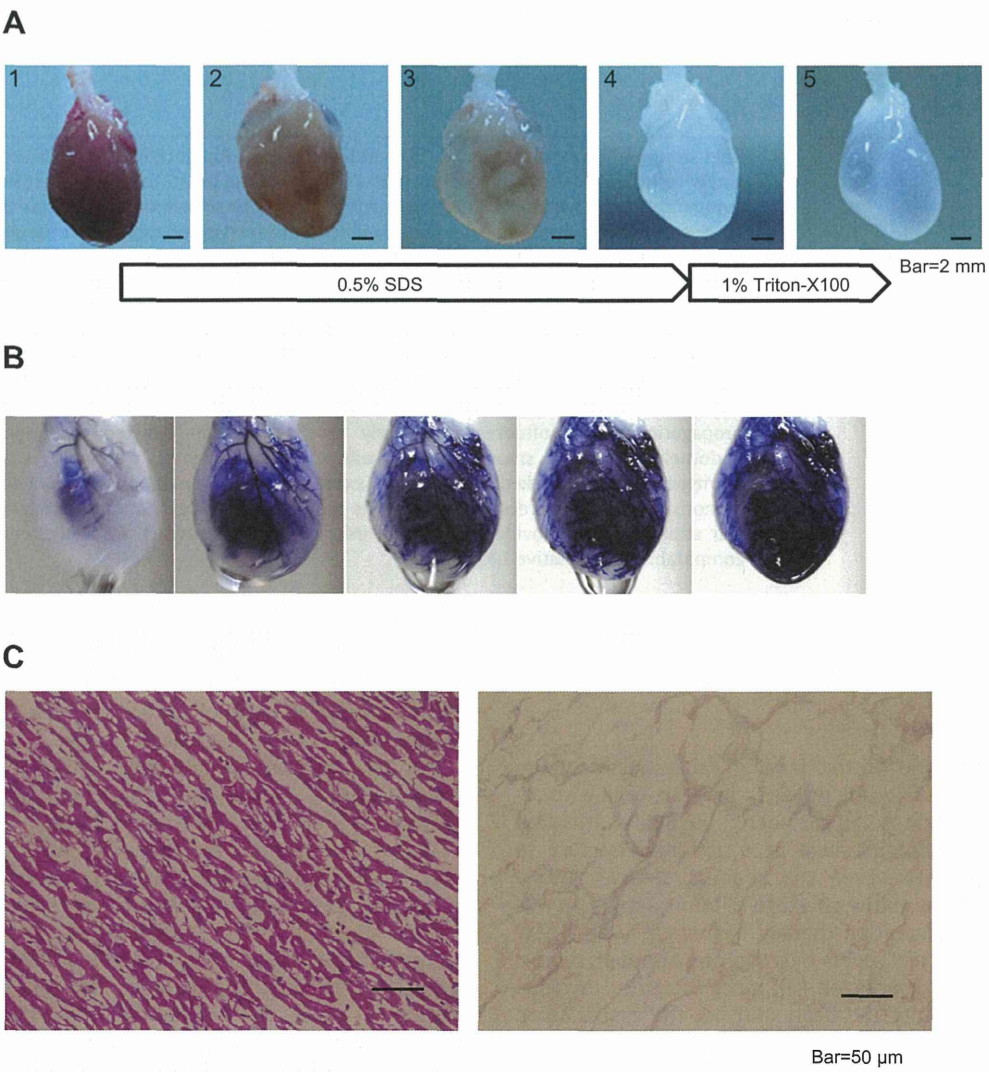

Fig. 1. Decellularization of rat hearts. (A) Macroscopic images of rat hearts during decellularization procedure: before decellularization (1); during 0.5% SDS solution perfusion (2–3); after overnight 0.5% SDS solution perfusion (4); after 1% TritonX-100 solution perfusion (5). Bars indicate 2 mm. (B) Visualization of the architecture of perfused coronary artery of decellularized extracellular matrix. (Evans blue solution was infused through aorta). (C) Microscopic structures of cadaveric (left) and decellularized (right) rat hearts (H–E staining). No nuclear staining was observed in decellularized extracellular matrix. Bars indicate 50 μm.

(Invitrogen), and EGM-2 Single Quots (CC-4176, Lonza) except FBS and GA-1000. Seeded cells consisting of cardiomyocytes, fibroblasts, and endothelial cells were infused through a T-shaped stopcock placed in the line. Recellularized rat hearts were perfused continuously and maintained in 5% CO_2 atmosphere. The culture medium was first changed at day 2 or day 3 with M199 (Invitrogen) containing 10% FBS (BioWest), 100 U/mL penicillin (Invitrogen), 100 μg/mL streptomycin (Invitrogen), and 10 μM cytosine arabinoside (Sigma–Aldrich), but without growth factors and then every 48–72 h.

2.5. Histology and immunofluorescence

We fixed rat cadaveric hearts, decellularized hearts, and recellularized hearts with 4% paraformaldehyde and cryosectioned them. This was followed by hematoxylin–eosin staining and immunostaining. We permeabilized the slides with 0.25% TritonX-100 for 20 min and blocked slides with PBS containing 10% BSA and 0.1% TritonX-100 for 60 min at RT. The samples were incubated overnight at 4 °C with the following primary antibodies: anti-sarcomeric alpha actinin antibody (mouse monoclonal 1:500; Abcam, Cambridge, UK), anti-sarcomeric alpha actinin

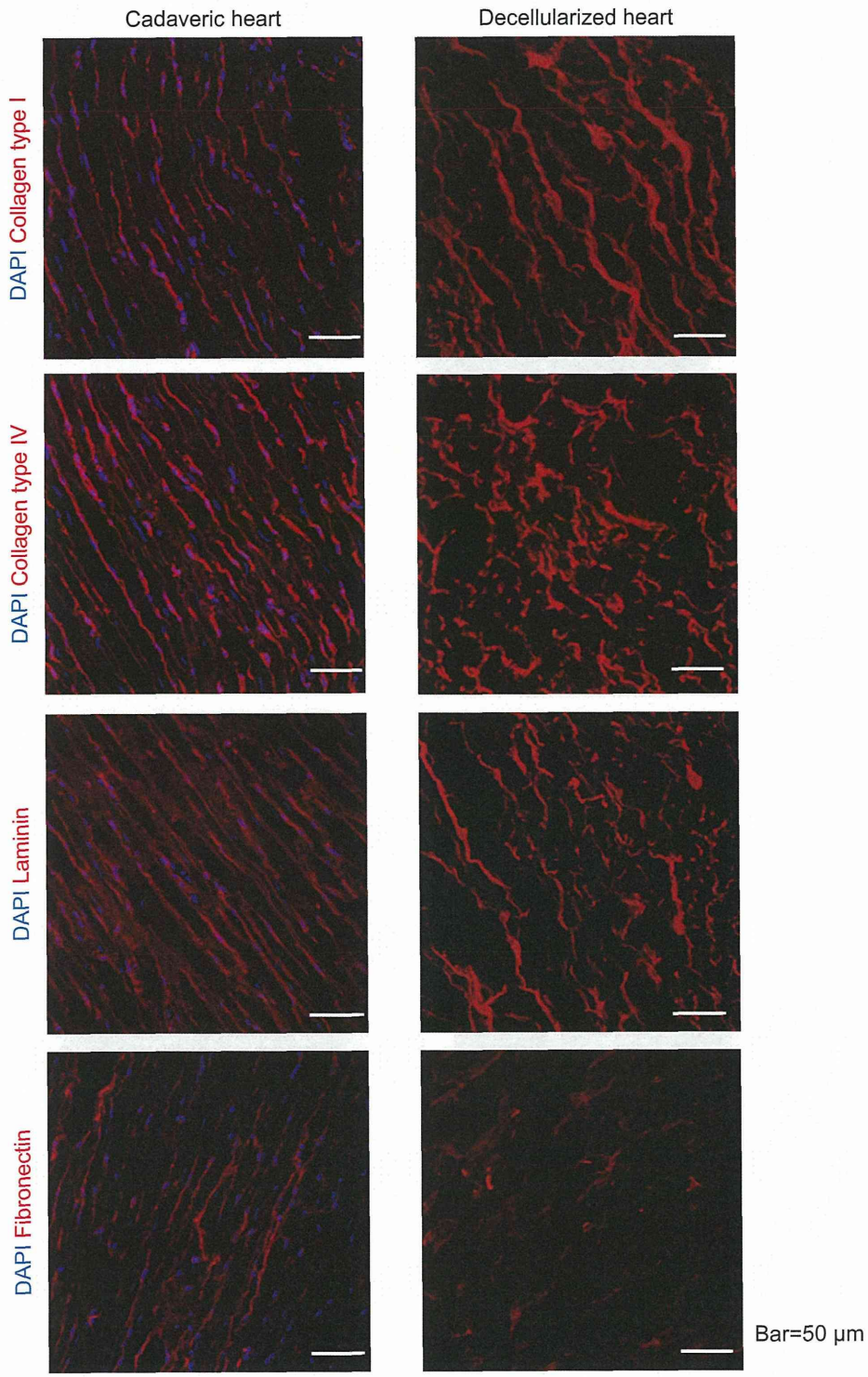

Fig. 2. Immunofluorescent staining of ECM in cadaveric and decellularized rat hearts. Collagen type I, collagen type IV, laminin, and fibronectin were maintained in decellularized (right) rat hearts as in cadaveric (left) hearts, but no nuclei was stained in decellularized (right) rat hearts. Bars indicate 50 μm.

antibody (rabbit polyclonal 1:100; Abcam), anti-laminin antibody (rabbit polyclonal 1:200; Abcam), anti-fibronectin antitibody (rabbit polyclonal 1:200; Abcam), anti-collagen IV antibody (rabbit polyclonal 1:200; Abcam), anti-collagen I antibody (rabbit polyclonal 1:200; Abcam), anti-connexin43 (Cx43) antibody (rabbit polyclonal 1:200; Invitrogen), anti-CD31 antibody (mouse monoclonal 1:100; Abcam), and anti-actin, alpha-smooth muscle-Cy3™ antibody (mouse monoclonal 1:500; Sigma–Aldrich). The samples were then incubated for 1 h with a 1:200 dilution of appropriate secondary antibodies. We embedded the samples in mounting medium containing DAPI (ProLong® Gold Antifade Reagent with DAPI; Invitrogen). Immunofluorescence images were acquired using a microscope (FSX: Olympus, Tokyo, Japan; Biorevo: Keyence, Osaka, Japan).

2.6. Western blot analysis

The frozen samples of an adult rat heart and engineered hearts were homogenized, and proteins were extracted on ice in a buffer solution containing 0.15 M NaCl, 1% NP-40, 50 mM Tris–HCl (pH 8.0), 0.5% sodium deoxycholate, 0.1% SDS and a cocktail of protease inhibitor (Complete, Mini, EDTA-free, Roche, Basel, Switzerland) and phosphatase inhibitor (PhosStop, 20 Tablets, Roche, Basel, Switzerland). Total protein (10 μg/lane) was electrophoresed and separated on an Extra PAGE One Precast Gel (nacalai tesque, Kyoto, Japan). After separation, proteins were transferred onto nitrocellulose membrane sheets (GE Healthcare Japan, Tokyo, Japan). Following transfer, the membrane was blocked in 5% low-fat dry milk in TBS-T at RT for 1 h. Then, the membrane was incubated at 4 °C overnight with following primary antibodies: sarcomeric alpha actinin (mouse monoclonal 1:500; Abcam), myosin heavy chain (MYH) (rabbit polyclonal 1:500; Santa Cruz, Dallas, TX, USA), cardiac troponin I (rabbit polyclonal 1:1000; Abcam), Cx43 (mouse monoclonal 1:1000; Invitrogen), VE-cadherin (goat polyclonal 1:500; Santa Cruz) or GAPDH (rabbit monoclonal 1:5000; Cell Signaling Technology, Danvers, MA, USA). Immunoreactive bands were visualized using an enhanced chemiluminescence (ECL) detection system (Pierce Western Blotting Substrate Plus, Thermo Fisher Scientific, Waltham, MA, USA) and an image analyzer (ImageQuant LAS 4000mini, GE Healthcare Japan).

2.7. Transmission electron microcopy

Decellularized and recellularized hearts were fixed using 2.5% glutaraldehyde (Wako, Osaka, Japan) in 0.1 M phosphate buffer (pH 7.4) through coronary perfusion; they were sectioned into 1-mm pieces and placed in 2.5% glutaraldehyde solution for 2 h. The samples were post-fixed with 1% osmium tetroxide and dehydrated with ethanol. They were embedded in epoxy resin and sectioned into 80 nm slices by

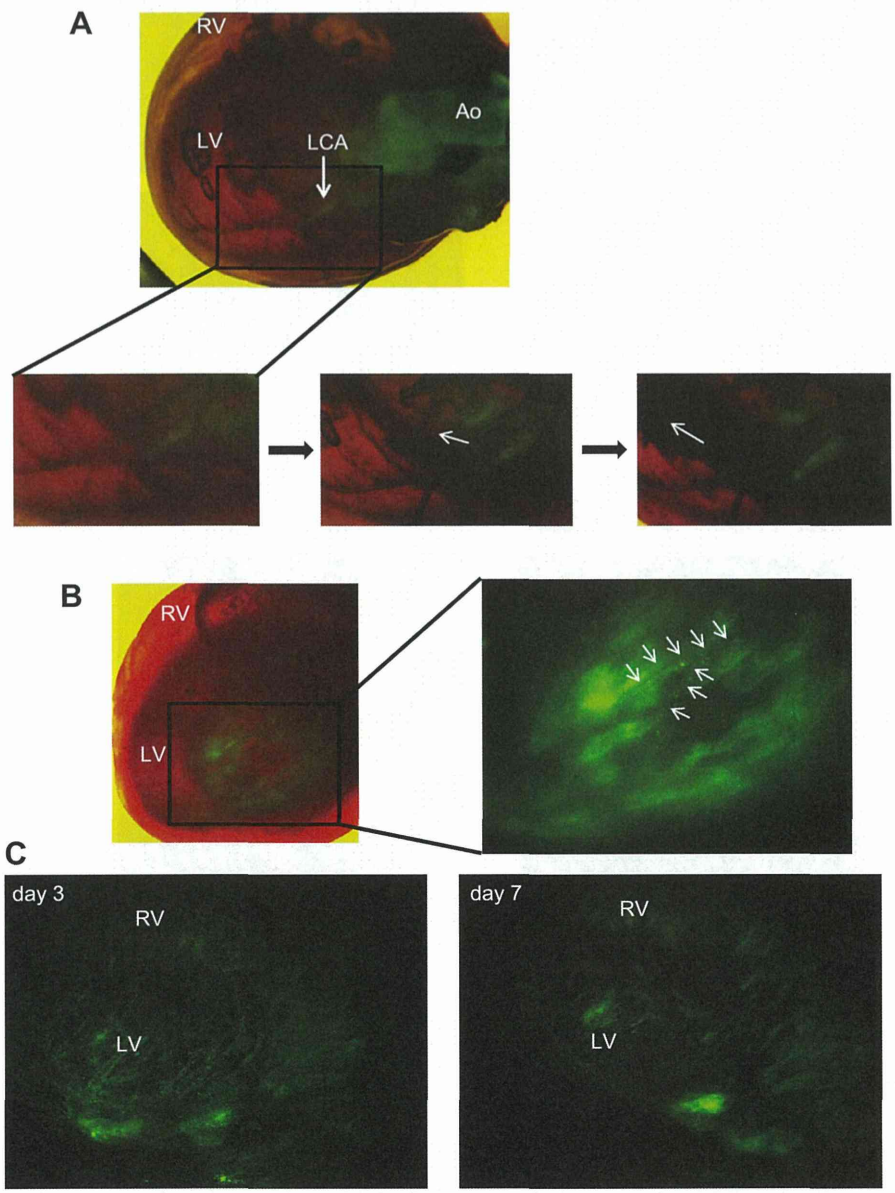

Fig. 3. Extravasation of GFP-labeled neonatal rat cardiac cells. (A) Dispersion of GFP-labeled isolated cardiac cells. GFP-labeled cells were antegradely infused into the coronary artery through aorta (upper panel). Time course of the migration of the cells is shown in magnified images (lower panels): After injection: 4 min (left), 11 min (middle), 16 min (right). The GFP-labeled cells (arrows) migrated into the interstitial spaces through extravasation. (B) At day 2, substantial portion of the seeded cells was observed in the interstitial spaces. Arrows show decellularized vessel structure. The seeded cells existed in the interstitial matrix as well as in the lumens of coronary arteries. (C) GFP-positive cells were retained in the heart for 7 days. Day 3 (left) and day 7 (right). GFP-positive cells were observed throughout the heart but inhomogeneously.

ultramicrotome. Ultra-thin sections were prepared and examined under an electron microscope (H-7650, Hitachi, Tokyo, Japan).

2.8. Transfection of adenovirus encoding GFP and GCaMP2

Isolated neonatal rat cardiac cells were infected with adenovirus encoding GFP and GCaMP2 [31] at a multiplicity of infection (m.o.i.) of 10 and 20, respectively. GFP and GCaMP2 expressing cardiac cells were suspended with the culture medium and injected into the decellularized hearts as described above.

2.9. Electrical and mechanical experiments

Electrocardiograms (ECGs) were recorded in epicardial surface of ventricle. Signals were then digitized through an AD converter (Digidata 1320, Molecular Devices, Sunnyvale, CA, USA) and analyzed with softwares (Axoscope, Molecular Devices; OriginPro, OriginLab Corporation, Northampton, MA, USA). Intraventricular pressures were recorded through a catheter (1.4Fr-Mikro-Tip™ Catheter Transducer, Millar, Bella Vista, NSW, Australia) with an amplifier (PowerLab, AD Instruments Inc., Dunedin, New Zealand).

2.10. Live tissue imaging

We observed recellularized hearts temporarily under a fluorescent stereomicroscope (Leica Microsystems Ltd., Wetzlar, Germany). Recellularized hearts were placed in culture flasks and their fluorescent images were recorded with a GFP-band path filter. Data analysis was performed using custom MALTAB software (MathWorks, Natick, MA, USA). Before fixation, calcium transient (CaT) of the recellularized hearts were optically recorded using a high-resolution CMOS camera (MiCAM02, Brainvision, Tokyo, Japan). Data analysis was performed using custom-made software (BV_Ana, Brainvision). Fast Fourier Transform (FFT) analyses were conducted using software (OriginPro, OriginLab Corporation).

3. Results

3.1. Decellularization of adult rat hearts

Perfusion of 0.5% SDS and subsequent application of 1% Triton-X100 removed all the cellular components from the hearts, leaving behind the extracellular matrices (Fig. 1A). Histological

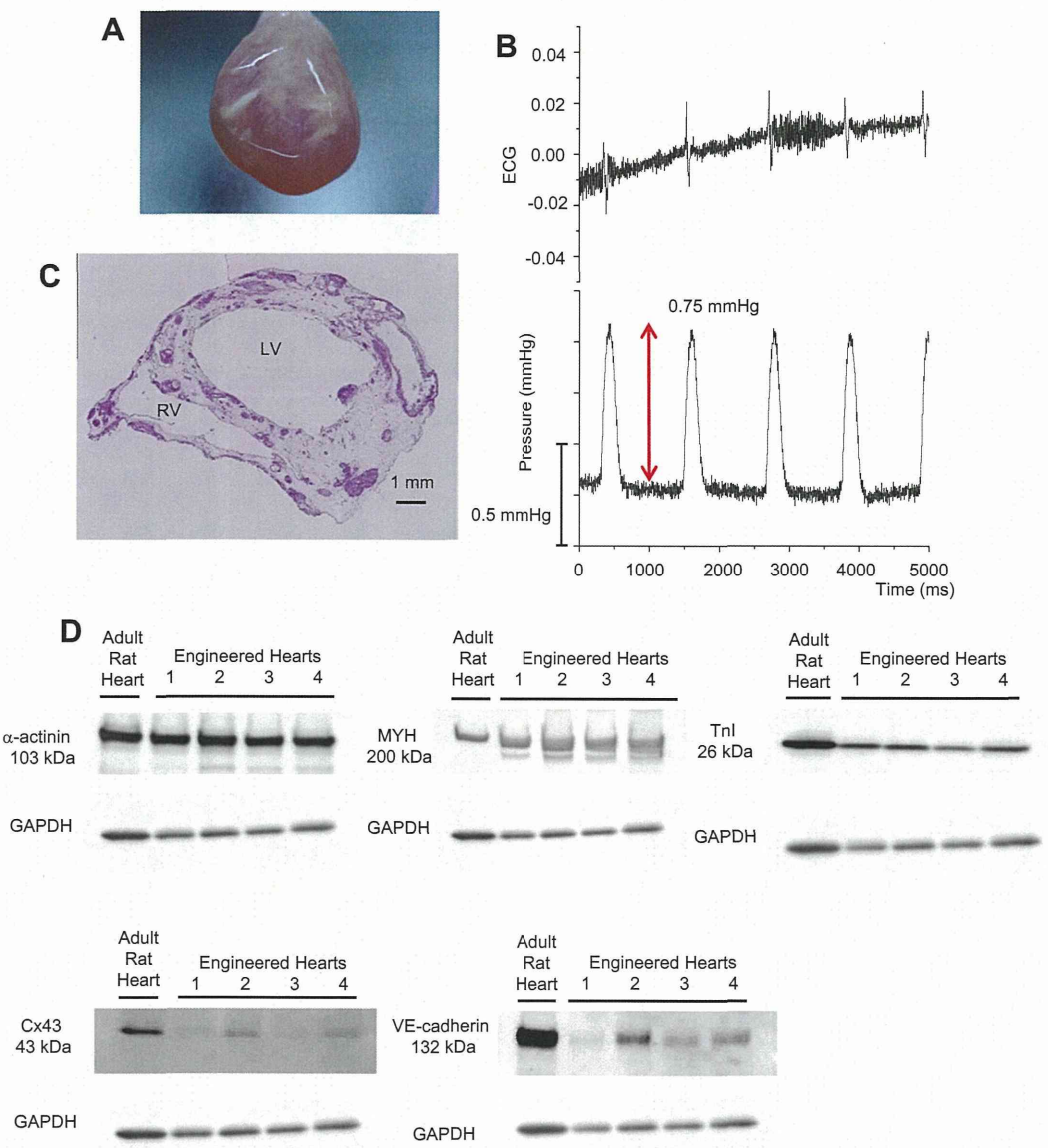

Fig. 4. Properties of recellularized hearts. (A) An image of a recellularized rat heart showing spontaneous beating. (Supplemental movie is available as Movie S2). (B) Real-time tracings of ECG and ventricular pressure are shown. The tracings of ECG and manometry were synchronized and intraventricular pressure was approximately 0.75 mmHg. (C) A microscopic image of a recellularized rat heart in transverse section (H–E staining). Inhomogeneous distribution of seeded cells was observed throughout the heart. Bar indicates 1 mm. (D) Western blot analysis of heart extracts. An adult rat heart and 4 engineered hearts were subjected to western blot analysis. Note the faint expression of VE-cadherin and connexin43 (Cx43) in engineered hearts compared to adult rat heart, in contrast to the abundant expression of sarcomeric alpha actinin, myosin heavy chain (MYH) and cardiac troponin I (TnI), both in engineered and native adult rat hearts.

evaluation revealed an absence of nuclei in the decellularized hearts (Figs. 1C and 2). Immunofluorescent staining demonstrated that collagen I, collagen IV, laminin, and fibronetin remained within the decellularized heart matrix (Fig. 2). Antegrade coronary perfusion with Evans blue dye delineated the extracellular structures of the main coronary arteries (Fig. 1B). The arterial remnants were abruptly terminated. Detailed observation revealed that decellularization procedure destroyed the entire vessel walls in the peripheral arterioles but not in the proximal arteries. This finding may be attributed to sparse extracellular matrices in the peripheral arterioles.

3.2. Whole-heart engraftment of GFP-labeled cells

Live tissue fluorescence imaging of the GFP-labeled seeded cells after antegrade infusion through coronary arteries revealed that the GFP-labeled cardiac cells had extended through the lumens of decellularized coronary arteries into the interstitial spaces at the tip of the remnant coronary arteries (Fig. 3A and Supplementary Movie 1). At day 3, inhomogeneous distribution of the GFP-positive cells was observed throughout the heart tissues. The seeded cells were found in the lumens of coronary arteries as well as in the interstitial matrix (Fig. 3B, C). We also observed that the GFP-positive cells were retained in the heart during the entire observation period (Fig. 3C).

Supplementary video related to this article can be found at http://dx.doi.org/10.1016/j.biomaterials.2014.05.080.

3.3. Recellularization of the decellularized hearts with cardiac cells of neonatal rats

We seeded decellularized rat hearts with freshly isolated neonatal cardiac cells through antegrade coronary perfusion. As the cell isolation procedure did not include techniques such as "pre-plating" method to remove specific cardiac cell types, both cardiomyocytes and other types of cells such as fibroblasts were seeded into the decellularized heart. The 3D organ-like culture was maintained for 8–30 days. Recellularized hearts started spontaneous contraction 2–3 days after recellularization, which continued for 8–30 days (Fig. 4A and Supplementary Movie 2). We

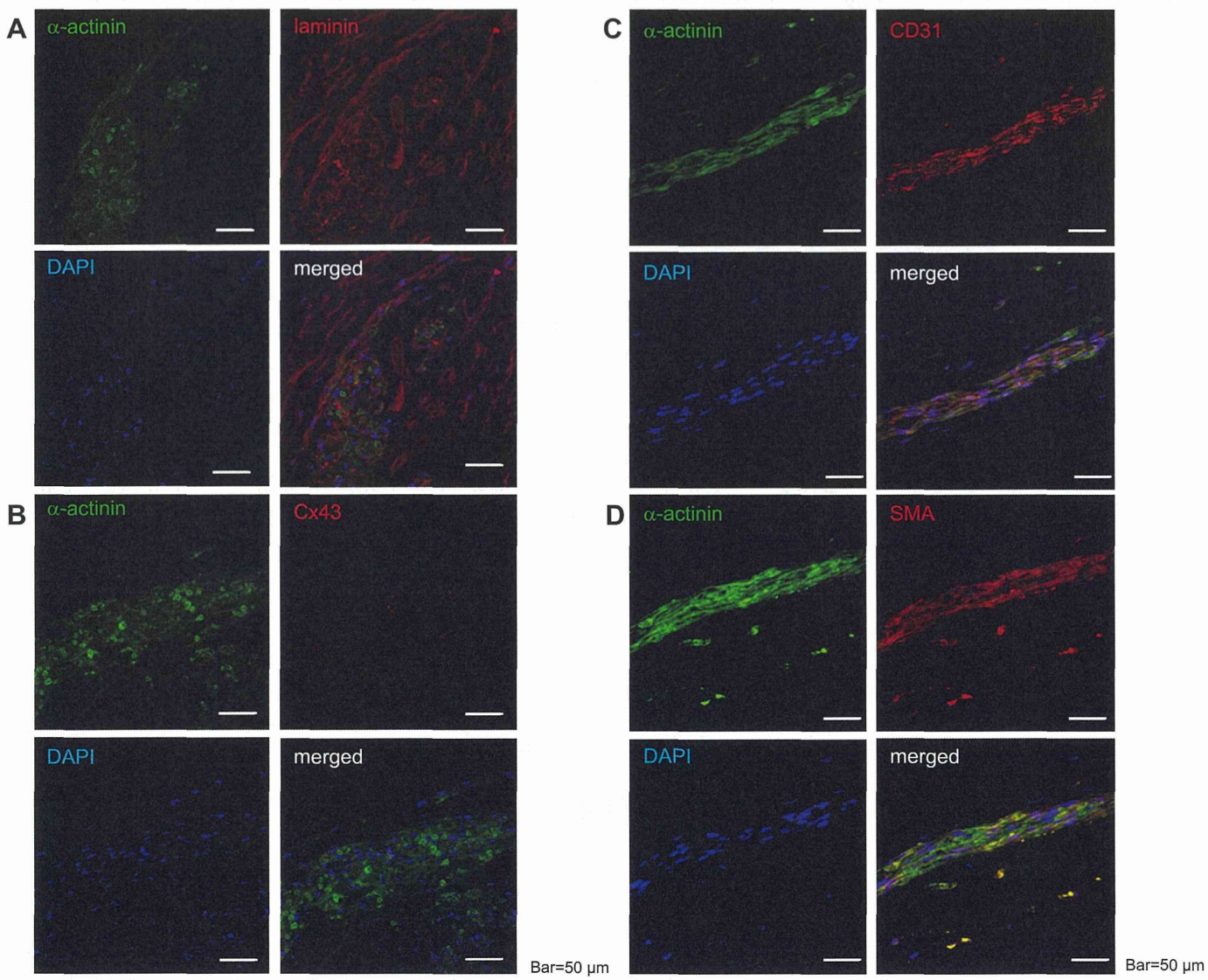

Fig. 5. Immunofluorescence study of recellularized hearts. (A) Sarcomeric alpha actinin-positive cells were surrounded by laminin-positive ECM. (B) Cx43 was sparsely observed among sarcomeric alpha actinin-positive cells. (C), (D) Random alignment of cardiomyocytes, endothelial cells, and smooth muscle cells. The mixture of different cells was observed. Alpha-actinin, CD31, and smooth-muscle-actin were used as cardiac, endothelial, and smooth muscle cell markers, respectively.

recorded electrocardiogram (ECG) and intraventricular pressure. The synchronized tracings of ECG and pressure were shown in Fig. 4B. Microscopic observation revealed that seeded cells adhered inhomogeneously to the decellularized ECM (Fig. 4C). We further examined whether cardiac proteins existed in recellularized hearts by western blot analysis (Fig 4D). As a result, cardiac contractile proteins, including sarcomeric alpha actinin, MYH and cardiac troponin I (TnI), were abundantly observed, while VE-cadherin and Cx43 were only faintly detected in engineered hearts compared to an adult rat heart. Among the seeded cells, sarcomeric alpha actinin positive cells were detected in the ventricles; these cells were surrounded by laminin-positive ECM (Fig. 5A). Although regions of the alpha actinin-positive cells were accompanied by Cx43, the expression was faint, which indicated that intercellular conduction might be immature as compared to adult hearts (Fig. 5B). An immunofluorescence study revealed a randomly-mixed alignment of cardiomyocytes, endothelial cells, and smooth muscle cells stained with alpha actinin, CD31, and smooth muscle (sm)-actin, respectively (Fig. 5C, D). CD31-positive cells and sm-actin-positive cells were not necessarily localized to decellularized vessel-like structures. Transmission Electron Microscope observations showed that the decellularized hearts preserved collagen fibers well in the ECM (Fig. 6A) and the recellularized hearts demonstrated the presence of sarcomeric structures surrounded by ECM (Fig. 6B).

Supplementary video related to this article can be found at http://dx.doi.org/10.1016/j.biomaterials.2014.05.080.

3.4. Excitation-propagation of recellularized hearts

Engineered hearts seeded with GCaMP2-expressing cardiac cells showed spontaneous beating within 2–3 days after recellularization, at which point they were subjected to optical imaging experiments. We observed that spontaneous excitations were generally well aligned and stably propagated in the engineered heart tissues (Fig. 7A and Supplementary Movie 3). Fig. 7A shows the representative images of propagation sequences in an engineered heart. Excitation seemed to emerge in the lateral wall of left ventricle (LV) and propagated through the free LV wall. Isochrone map of the propagating CaT suggested inhomogeneous conduction in substantial areas (Fig. 7C). Conduction velocity (CV) was an order of magnitude or slower (approximately 0.5–5 cm/s) compared to normal adult rat hearts.

Supplementary video related to this article can be found at http://dx.doi.org/10.1016/j.biomaterials.2014.05.080.

3.5. Arrhythmogenicity of recellularized heart tissues

To examine the underlying mechanisms of arrhythmogenesis in the engineered heart tissues and the time-course of maturation in electrical properties, live tissue fluorescence video imaging was employed. We used FFT analysis to examine the synchronicity. Spontaneous excitation of CaT recorded at the three discrete points in the engineered heart tissues were subjected to FFT analysis. In the sample of the first group, during spontaneous beating, the

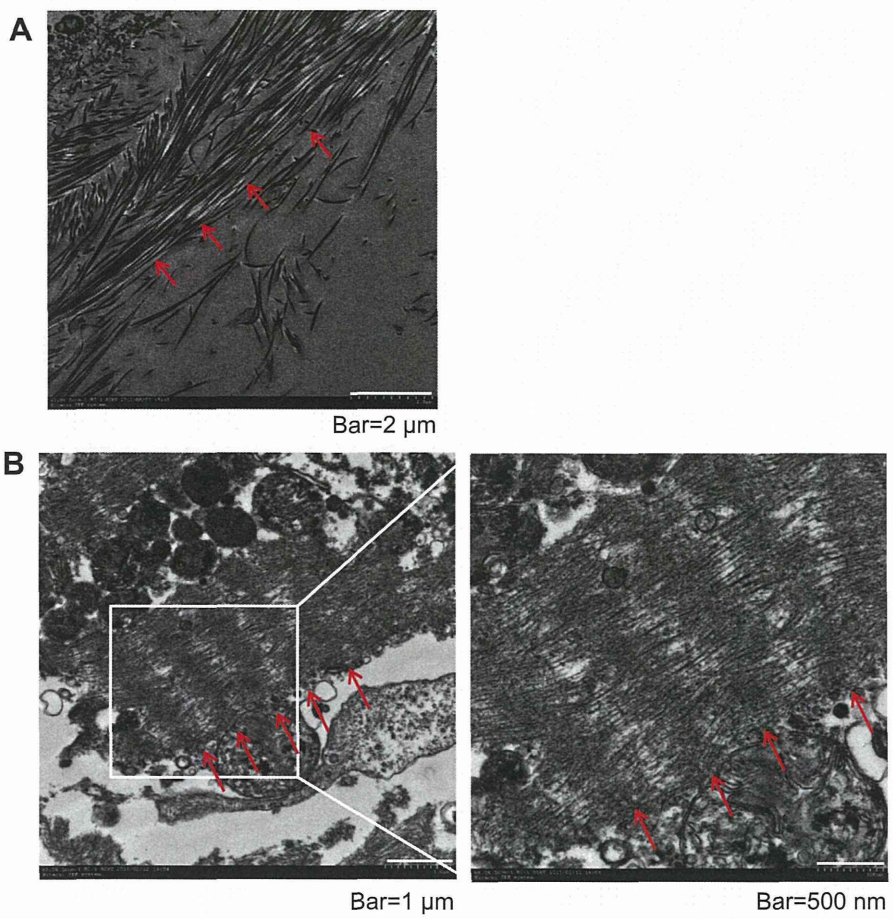

Fig. 6. Ultrastructure of decellularized and recellularized rat hearts by transmission electron microscopy. (A) Ultrastructure of a decellularized heart. Collagen fibers (arrows) in the ECM were well preserved after decellularization procedure. (B) Ultrastructure of a recellularized heart. Arrows show cells with well-organized stria. Cardiac cells seemed to be surrounded by ECM.

entire heart tissues were well-synchronized (Fig. 8A–E and Supplementary Movie 4). Isochrone map showed that excitation propagated rapidly through the left ventricle (Fig. 8D). Frequency analysis showed similar frequency profile pattern at each point (Fig. 8E). On the other hand, in the sample of the second group, although substantial parts of the tissues showed well-organized propagation of excitation, unsynchronized beatings were also observed around ROI-2 (Fig. 9A–E and Supplementary Movie 5). Isochrone map of the propagating CaT showed that initial activation generated from two distinct sites at basal and apical parts of the heart (Fig. 9D). The frequency profiles were accordingly similar at ROI-1 and ROI-3, but not at ROI-2 (Fig. 9E). These observations suggested that there were multiple re-entry like circuits. The sample of the third group exhibited markedly arrhythmogenic characteristics. The heart tissues showed spontaneous contraction, but each region did not show synchronization (Fig. 10A–E and Supplementary Movie 6). Conduction between left and right sides of the heart was hardly observed (Fig. 10D).

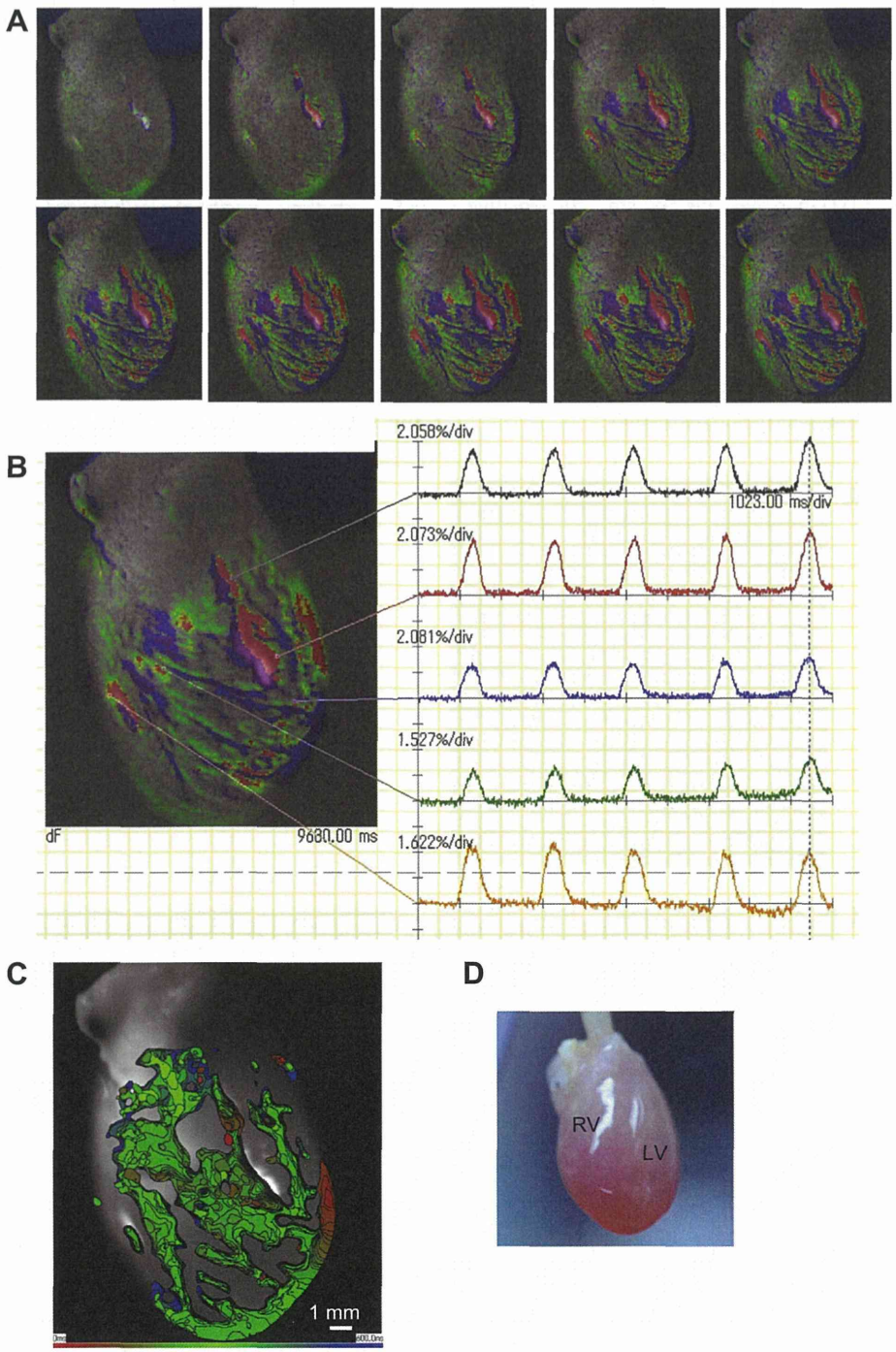

Fig. 7. Propagation of the intracellular calcium transient (CaT) in a recellularized heart. (A) Sequential images in spontaneous beating (every 40 ms). Optical images showed excitation-propagation throughout epicardial surface of the recellularized heart. (B) Detection of the intracellular CaT. (C) Isochrone map (in 10 ms color-coded intervals) of the propagating CaT. Isochrone map suggested inhomogeneous propagation in substantial areas. (D) Anatomical features of the recellularized heart from a frame of video file.